Uptake of ammonium and nitrate by calcium carbonate polymorphs

Rinat I. Gabitov [1*], Peter M. Wynn [2], Catherine Wearing[2], Logan Carlson [3], Gombojav Ariunbold [3], Angel L. Jimenez-Arroyo [4], Elizabeth Bell [5,] Nathan Halcovitch [6], Rooban VKG Thirumalai[7], EIMF[8]

[1] Department of Geosciences, Mississippi State University (MSU), USA
[2] Lancaster Environment Centre, Lancaster University, UK
[3] Department of Physics and Astronomy, Mississippi State University, USA
[4] Department of Chemistry, Geosciences & Physics, Tarleton State University, USA
[5] Department of Earth, Planetary, and Space Sciences, University of California, Los Angeles (UCLA), USA
[6] Department of Chemistry, Lancaster University, UK
[7] Institute for Imagining and Analytical Techniques, Mississippi State University, USA
[8] Edinburgh Ion Microprobe Facility, Institute of Earth Science, School of Geosciences, University of Edinburgh, EH9 3JW, UK
* Correspondence: Rinat Gabitov, rg850@msstate.edu

Abstract

The abundance of nitrogen ionic species in natural waters is linked to drivers of environmental change at the global and local scales throughout the anthropogenic era. The potential for calcium carbonate minerals as a resistant host material to record the reactive nitrogen composition of natural waters is driving a requirement to understand incorporation mechanisms and to develop absolute analytical techniques that operate at the μm scale. To assess the capability of calcium carbonate for the uptake of dissolved nitrogen compounds, we conducted an experimental study on the incorporation of ammonium and nitrate into inorganic carbonate crystals. Calcium carbonate polymorphs were synthesized in nitrogen-containing growth media and were used to quantify nitrate and ammonium uptake by calcite, aragonite, and vaterite phases. Automated colourimetry analyses yielded partition coefficients between mineral and fluid ranging from ($D(NO_3)$) of $2.12 \cdot 10^{-2}$ to $6.51 \cdot 10^{-1}$ regardless of $CaCO_3$ polymorph (i.e. calcite and aragonite). Secondary ionisation mass spectrometry (SIMS) demonstrated ammonium is more readily incorporated into polymorphs of vaterite and aragonite ($D(NH_4) = 8.77 \cdot 10^{-3}$ and $D(NH_4) = 1.63 \cdot 10^{-2}$, respectively), as opposed to calcite ($D(NH_4) = 3.09 \cdot 10^{-3}$). SIMS was also used to assess the degree of nitrogen heterogeneity within crystal phases. Calcite rhomboids were found to have high internal heterogeneity, with an almost two orders of magnitude shift in N concentration due to inferred sectoral zoning. The polycrystalline nature of aragonite spherulites mitigated intra-spherulite heterogeneity, resulting in analytical repeatability of <10 % standard deviation (1 s.d.) when $N_{(CaCO3)}$ = 164–169 ppm. Inter-spherulite variability for aragonite polymorphs was calculated to average 7.6 % (1 s.d.), thus demonstrating a potential for development of reference materials for high precision analytical techniques. Despite the heterogeneity observed across the various synthesized $CaCO_3$ polymorphs, the technique appears to have potential for use as a SIMS calibration dataset and for estimating absolute nitrogen concentrations in the carbonate palaeorecord at the μm scale.

Keywords: ammonium, nitrate, calcite, aragonite, vaterite.

1. Introduction

Nitrogen is a major element in the atmosphere,biosphere and hydrosphere which has been extensively impacted byanthropogenic activity, e.g., fertilizer use and industrial

atmospheric pollution. This has had profound consequences for the reactive part of the nitrogen cycle, with negative environmental impacts on freshwater and marine ecosystems as well as impacting human health through nitrate contamination of groundwater and drinking water supplies (e.g., Vitousek et al., 1997; Galloway et al., 2008; Ma et al., 2021; Matiatos et al., 2021). The strong affiliation of nitrogen with anthropogenic activity makes it one of the key markers of the Industrial Era (e.g., Dean et al., 2014).

Currently, there are few high-resolution, globally distributed palaeorecords of nitrogen dynamics, and a distinct lack of knowledge regarding the suitability of host materials capable of preserving such a record throughout the anthropogenic era. Host materials must provide resistance to changes in the redox state and the chemical form of the nitrogen preserved. Carbonate records are thought to preserve such information on environmental nitrogen concentrations and isotope compositions (in both organic and inorganic forms), allowing nitrogen to be traced to source and changes detected through time. Example carbonate records include speleothem calcite which has been used to record ground water nitrate dynamics (Wynn et al., 2021); foraminifera shells which have been used to study fluxes of intertidal nitrogen (Glock et al., 2019); and coral aragonite for understanding marine pollution and nutrient concentration changes (e.g., Yamazaki et al. 2013).Vaterite, a third $CaCO_3$ polymorph, which occurs as a biogenic mineral in fish otoliths (e.g., Wood et al., 2022) is frequently used to reconstruct fish migration history (e.g., Lueders-Dumont et al., 2022). In this study, we investigated inorganic nitrogen uptake in complex ionic forms.

Experimental data on nitrogen incorporation into calcium carbonate minerals is lacking, and quantitative analysis at high spatial resolution has remained largely beyond reach due to a lack of appropriate reference materials that are matrix-matched to carbonate host samples. To date, the incorporation modes of nitrate and ammonium into $CaCO_3$ remains unclear. The charge balance requirements for replacing divalent Ca^{2+} and CO_3^{2-} with monovalent NH_4^+ and NO_3^- ions mean that both replacements need to occur simultaneously to maintain the charge neutrality of calcite. Although ionic radii (r) of NO_3^- and CO_3^{2-} are similar (1.79 and 1.78 Å), the large ionic radii of $r(NH_4^+)$ =1.37 Å compared to $r(Ca^{2+})$=1.00 Å is expected to limit ammonium incorporation (Shannon, 1976; Jenkins and Thakur, 1979; Wiredchemist, 2021). Alternative mechanisms of interstitial incorporation are linked to crystal defects, where high defect density promotes impurity uptake. To date, experimental data on the mechanism of nitrogen uptake by $CaCO_3$ are restricted to adsorption studies (e.g., Hofmann et al., 2016), which found a strong affinity of nitrate to calcite surfaces, or qualitative characterization studies of nitrate-bearing calcites (e.g., Kontrec et al., 2004) that showed that addition of nitrate does not have an effect on X-ray powder diffraction (XRPD) patterns or distortion of the calcite lattice from axial symmetry. Here, to quantify the uptake of nitrate and ammonium by $CaCO_3$, we evaluated their partition coefficients between calcite, aragonite, vaterite, and aqueous growth media. We also used ion microprobe (SIMS) to assess the relative heterogeneity of individual polymorphs produced in these growth experiments. These analyses offer preliminary insight into possible mechanisms of anion incorporation and contribute to the early stages of developing calibration references that may enable quantification of nitrogen in the palaeorecord at the micrometre scale.

2. Experimental and analytical methods

2.1 Crystallization experiments

The methodology used in this study for the precipitation of calcite crystals was initially developed by Gruzensky (1967) and subsequently modified by several studies (e.g., Paquette and Reeder, 1995; Gabitov et al., 2014, 2021). The principle of the method relies upon the decomposition of ammonium carbonate to produce CO_2 and NH_3 gas, followed by diffusion into an NH_4Cl-$CaCl_2$ solution. This promotes the growth of calcium carbonate crystals up to a

few mm in size. The experimental setup is depicted in Figure 1. Five different crystal growth experiments were set up (labelled SIMS-1 to SIMS-5), each containing an NH_4Cl-$CaCl_2$ solution in varying concentration (Table 1). Ammonium concentration varied from 0.016 to 4M. A calcium concentration of 0.01 M was used in all experiments except SIMS-5, where a higher Ca content (0.02 M) was required for saturating the solution with respect to calcite (Zhao et al., 2015). Four additional experiments (labelled SIMS-6 to SIMS-9), with similar NH_4Cl-$CaCl_2$ concentration but different nitrate nitrogen (NO_3-N) levels varying from 0 to 100 ppm were conducted (Table 1). Carbonate crystals grew on the walls and the bottom of the flask, as well as at the solution-air interface. The time taken to reach the onset of crystallization was determined by visual observation of crystals on the walls of the flask, and the duration of growth was allowed to vary between 1.5 to 4 months. At the end of the experiments, the NH_4Cl-$CaCl_2$ fluids were analysed for nitrate and ammonium concentration. Solids were removed from the flask, rinsed with (DI) Mili-Q water at least three times, dried, visually characterized for their crystal structure, separated into rhomboids versus spherulite and truncated pyramid morphologies using optical microscopy, and analysed for nitrate and ammonium content. Experimental parameters are presented in Table 1.

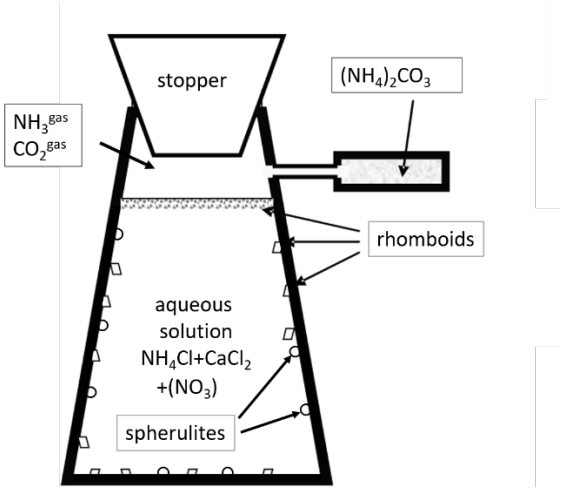

Figure 1. Experimental setup. Crystals of $CaCO_3$ grew in $NH_4Cl+CaCl_2$ solutions, occasionally doped with NO_3.

Table 1. Experimental setup

Name	NH_4Cl, mol/L	$CaCl_2$, mol/L	NH_4Cl, g/400ml	$CaCl_2*2H_2O$, g/400ml	NO_3-N ppm	NO_3-N, std, ml	t, days total	t, days cryst.
SIMS-1	0.016	0.010	0.3341	0.5734	0	0	51	49
SIMS-2	0.031	0.010	0.6680	0.5830	0	0	51	n/d
SIMS-3	0.13	0.010	2.677	0.5830	0	0	52	n/d
SIMS-4	1.0	0.010	21.35	0.5805	0	0	52	n/d
SIMS-5	4.0	0.020	85.57	1.181	0	0	115	n/d
SIMS-6	0.50	0.010	10.64	0.5698	0	0	42	34
SIMS-7	0.50	0.010	10.64	0.5790	1	0.4	42	34
SIMS-8	0.50	0.010	10.67	0.5973	10	4	42	34
SIMS-9	0.50	0.010	10.69	0.5958	100	40	42	34

All concentrations are for initial solutions and correspond to the amount of loaded chemicals or nitrate reference solution (1000 mg/L or 1000 ppm of N), where ppm are parts per million by volume. Total experimental duration and time passed since onset of crystallization are presented as t, days total; and t, days since onset of crystallization (cryst.), respectively. NO_3-N stands for nitrogen in nitrate; n/d is not determined, i.e., the day when crystals became visible was not recorded.

2.2 Optical microscopy, X-ray diffraction analyses, and Raman spectroscopy

Precipitated calcium carbonate crystals were examined using optical microscopy to determine their morphology and size. Three distinct crystal morphologies were identified: rhomboids, spherulites (hemispherical bundles of acicular crystals radiating from the centre), and truncated pyramids (only formed in experiments conducted at high ammonium concentrations). With the exception of SIMS-5, each experiment produced more than one of these morphologies. When possible, individual crystal shapes were separated with forceps for further characterization. A point counting assessment using ImageJ was conducted based on grains observed in the available scanning electron microscopy (SEM) images.

XRPD patterns were measured with a Rigaku SmartLab X-ray diffractometer with a 9-kW rotating anode Cu-source equipped with a high-resolution Vertical θ/θ 4-Circle Goniometer and D/teX-ULTRA 250 High-Speed Position-Sensitive Detector System in reflectance mode at Lancaster University, UK. The system was configured with parallel-beam optics and a Ge (220) 2 bounce monochromator on the incident side. Crystalline solid samples were ground in a pestle and mortar and were loaded onto an offcut Si (911) zero-background holder. The measurements were performed as θ/2θ scans with a step size of 0.01 degrees, and a scanning speed of 1.5 degrees per minute.

SEM images were collected using a JEOL JSM-6500F FE-SEM at the Institute for Imaging & Analytical Technologies (I^2AT), Mississippi State University (MSU). Samples were placed on SEM sample stubs containing a double-sided carbon tape and were coated with platinum (10 nm thickness). The instrument was operated at a voltage of 5.0 kV and a working distance varying from 17 to 37.5 mm.

Individual calcium carbonate crystals and spherulites were mounted on double-sided tape for in situ Raman spectroscopy at Mississippi State University, USA. All spectra were observed using a Civil Laser 532 nm DPSS laser and an Andor Shamrock SR-500i spectrograph with a 600 lines/mm grating. The spectra were then produced using the attached Andor Solus Software with the SR-500i in accumulation mode with 100 accumulations of 2 second scans. The laser power was also maintained at 6.0 mW for all scans. Raman spectra for rhomboids, spherulites, and truncated pyramids were collected by performing three scans across three different regions of each sample. During scanning, the sample was translated across the x-y plane and refocused along the z-axis to maximize the signal for each region. All data underwent background subtraction using airPLS (adaptive iteratively reweighted Penalized Least Squares) background fitting, with a smoothness parameter (lambda) of 50, a polynomial order of 2, and a maximum of 15 iterations (Zhang et al., 2010). In cases where negative values were present, the minimum value was subtracted to ensure all values remained positive before proceeding to the next step. Finally, the data were scaled by the maximum intensity of the spectra after background subtraction to generate relative raman spectra.

2.3 AQ-2 analyses for nitrate and ammonium

Nitrate concentrations in post-experimental products were analysed using automated colourimetry (instrument model AQ2 SEAL discrete analyser, method EPA 353.2) following procedures described in Wynn et al. (2021). The methodology (based on the cadmium reduction of nitrate to nitrite) has an upper analytical range of 5 mg/L (ppm) NO_3-N (nitrogen in nitrate) and a limit of detection (LOD) calculated as 0.01 ppm. Using the same sample

aliquots, concentrations of ammonia were determined, based on indophenol blue colourimetry (instrument model AQ2 SEAL discrete analyser, method EPA 350.1). The LOD for this technique was 0.02 ppm, with an upper range of 1 ppm NH_4-N (nitrogen in ammonium). For both techniques, samples were diluted to within the range of the calibration reference materials. Analytical precision based on the repeat analysis of reference materials (2.5 ppm and 0.5 ppm N for nitrate and ammonia analysis respectively) is reported to be within 5% of expected values.

For analysis of N in experimental solids, modifications to the analytical technique were as follows. Solid calcium carbonate samples were prepared for NO_3-N and NH_4-N analyses by dissolving 20 mg of $CaCO_3$ in 0.4 ml of ultra-pure 1M HCl and subsequently diluted using 0.6 ml of DI Milli-Q water. This produced a final chlorine concentration of 0.4 M. Due to the high sensitivity of the SEAL AQ-2 analyser to chlorine, samples derived from the acid dissolution of calcium carbonate were matrix-matched to reference materials. A zero-N carbonate matrix was prepared by dissolving 800 mg of nitrogen-free $CaCO_3$ in 16 ml of 1M HCl, followed by the addition of 24 ml of DI Milli-Q water. The obtained matrix was used in the preparation of reference solutions using a stock 1000 ppm N certified reference. Analysis of ammonia in the same samples and zero-N reference matrix were undertaken following further dilution by a factor of 5 to produce a final chlorine concentration of 0.08 M.

2.4 Ion microprobe analyses

Post experimental solids (rhomboids and spherulites) were embedded into cylindrical epoxy (Buehler EpoxyCure) mounts using double-sided sticky tape and 1-inch Teflon O-rings at Mississippi State University, USA. Mounts were flattened with 600, 800, and 1200 grit SiC paper, followed by polishing with 1µm alumina powder on a polishing cloth. After rinsing with DI water and drying, sample mounts were coated with 20 nm gold and examined with SIMS for nitrogen content. SIMS data are reported as the ratio of $^{12}C^{14}N$ to $^{12}C^{12}C$ (later referred to as CN/CC), which is proportional to total nitrogen in $CaCO_3$.

Preliminary scoping studies using an ion microprobe to detect N in calcite were undertaken using a CAMECA IMS 7f-GEO at the University of Edinburgh, School of Geosciences, UK. Due to interference between $^{12}C^{14}N$ and $^{13}C^{13}C$ at mass 26 and the limited mass resolving power of the instrument, a correction was applied to the measured signal. The $^{13}C^{13}C$ contribution was estimated using the natural isotopic abundance of ^{13}C, calculated as $^{12}C^{12}C \times 0.011$. The corrected $^{12}C^{14}N$ intensity was obtained by subtracting the calculated $^{13}C^{13}C$ signal from the total intensity at mass 26. Data acquired using the CAMECA IMS 7f-GEO are presented in the Supplementary Materials (File S1_Edinburgh ims-1270).

The data presented in this paper were collected at high mass resolving power at UCLA, using a CAMECA IMS 1290 instrument. Here, a 2 nA Cs^+ primary beam was focused to a ~10 µm spot and accelerated at 10kV to a sample stage held at -10kV. A normal incidence electron gun was used to compensate for charge buildup. The primary beam was rastered in a 25 × 25 µm square for 180 s to mitigate for, if any, surface contamination, after which measurements were made using a 5 × 5 µm raster. The measurements were made in monocollection mode employing the axial electron multiplier (EM) with an MRP ~7500 using an entrance slit width of 41 µm, exit slit of 130 µm, and field aperture width of 2000 µm. The masses analysed include $^{12}C^{12}C$ and $^{12}C^{14}N$ for 10 cycles. Each cycle lasted 12.5 s, which included waiting times of 4s on the 23.5 ("dummy mass") and 1s each on the $^{12}C^{12}C$ and $^{12}C^{14}N$. Counting times comprised 0.5s on the 23.5 ("dummy mass"), 2s on $^{12}C^{12}C$, and 4s on $^{12}C^{14}N$). The deadtime correction was 47.7 ns.

Nitrogen is more abundant in epoxy than in calcite (Table S-1). Therefore, potential contamination, which cannot be completely avoided, was evaluated for the experimental calcites. After 180 s of pre-sputtering on the natural (low-N) UCLA setup calcite, the $^{12}C^{14}N$ count rate decreased to $2 \cdot 10^2$ cps. In comparison, the experimental calcites exhibit CN count

rates at least six times higher: after identical pre-sputtering, the lowest-N experimental calcite showed $1.3 \cdot 10^3$ cps, and the highest-N sample reached up to $5 \cdot 10^5$ cps. Accordingly, we estimate that any contamination contribution is below 17% for the lowest-N experimental calcite and below 0.05% for the highest-N sample.

3. Results

3.1 Morphological characterization, bulk XRPD, and in-situ Raman spectroscopy.

Examples of loose rhomboids and spherulites are shown in reflected light microscopy images from experiments SIMS-1–4 (Figure 2 A–D). Rhomboids and spherulites selected from each sample (SIMS-1–4) were mounted in epoxy (ultimately for use with ion microprobe analysis) as shown in Figure 2 (E–H). Crystal images from other experiments (including truncated pyramids) are shown as photomicrographs in the supplementary materials (S2 and S3). The size of individual crystals and/or spherulites qualitatively increases upon progression through SIMS-1, 2, 3, 4, and 5, coeval with increasing ammonium concentration in the growth media (NH_4-$N_{(aq)}$) from 0.016 M to 4 M (Table 1). Crystal sizes in experiments SIMS-6–9 (NH_4-$N_{(aq)}$ = 0.5 M) were similar to those in SIMS-4 (NH_4-$N_{(aq)}$ = 1 M). Spherulites were observed in all experiments except SIMS-5. ImageJ analyses showed that the morphology proportions are as follows: SIMS-1, 60% rhomboids, 40% spherulites; SIMS-2, 100% rhomboids; SIMS-3, 94% rhomboids, 6% spherulites; SIMS-4, 85% truncated pyramids, 15% spherulites; SIMS-6, 22% truncated pyramids, 61% spherulites, 17% rhomboids. For SIMS-2, a value of 100% was assigned because no spherulites were observed in the available SEM image. However, spherulites were later found in experiment SIMS-2, when specifically searching for such a morphology. Overall, the observations presented below are generally consistent with the XRPD data (Table 2) regarding the percentages of calcite, aragonite, and vaterite.

The texture of spherulites is also different between experiments, as shown on SEM images (Figure 2 I–L). At lower ammonium concentration (experiments SIMS-1, 2, 3, 6, 7, 8, 9), spherulites consist of bundles of needle-shaped crystals radiating from the centre of each hemisphere (Figure 2 I–K). Such texture blocks light transmission through the spherulites (Figure 2 A, B) and changes the intensity of reflected light on polished spherulites, which look darker than calcites due to poor polishing compared to smooth calcite surfaces (Figure 2 E–G). This is not the case for sample SIMS-4 (experiment where spherulite precipitated at the highest ammonium concentration), where constituents of spherulites are more equant in shape, which causes partial light transmission (Figure 2D), slightly smoother/brighter surfaces (Figure 2H), and equant building blocks (Figure 2L) instead of radiating needles (Figure 2 I-K).

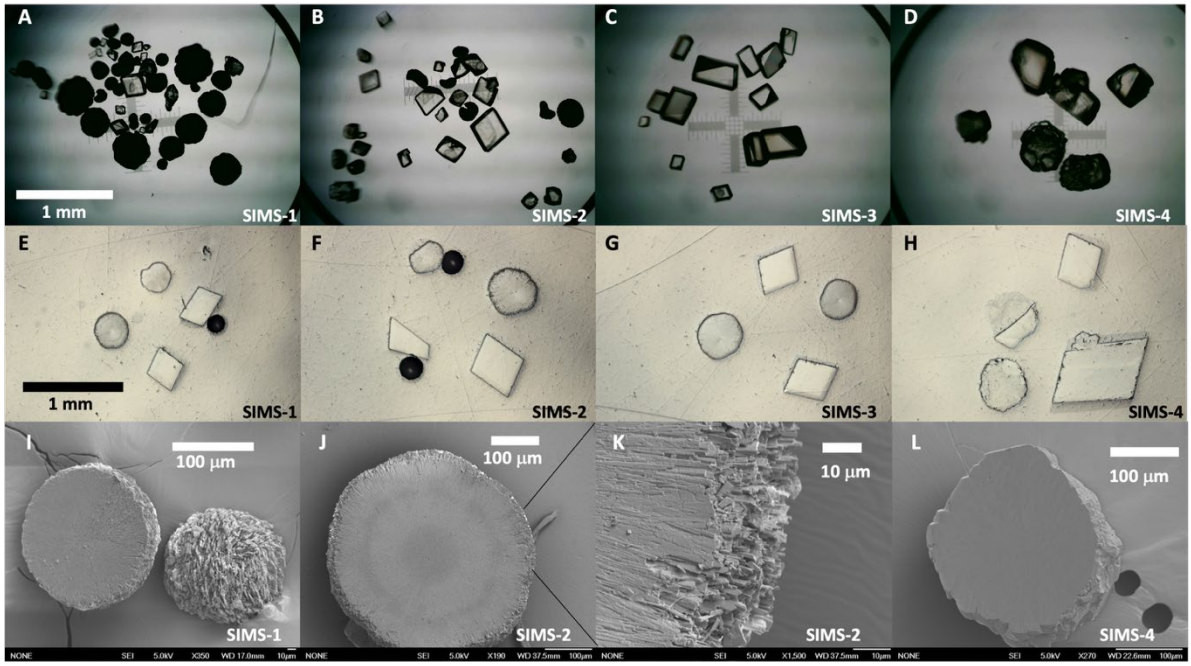

Figure 2. Example of optical SEM images of post-experimental solids. Transmitted light of loose crystals (A-D); reflected light of mounted and polished rhomboids and spherulites (E-H); SEM images of spherulites from experiments SIMS-1, 2, and 4 (I–L), the magnified rim of SIMS-2 spherulite is shown on Fig. 2K. Spherulites from experiment SIMS-3, 6, 7, 8, and 9 have textures identical to those of SIMS-2. Rhomboids in all experiments, as well as spherulites from experiment SIMS-4, are calcite. All other spherulites are aragonite, except those from SIMS-1, which are vaterite.

The obtained diffraction patterns from XRPD analysis showed that crystals from experiment SIMS-1 contain a mixture of calcite and vaterite (Table 2, Figure 3a), whereas in experiments SIMS-6, 7, and 8 the mixture comprised calcite and aragonite. Figure 3b shows an example of the diffraction pattern of the sample SIMS-6. XRPD revealed calcite as the only mineral phase in the remaining experiments (i.e., SIMS-2, 3, 4, 9), albeit subsequent Raman spectra at the scale of individual crystals identified spherulites of aragonite mineralogy in SIMS-2, 3, and 9. Raman spectra confirmed the spherulites in SIMS-4 to be of calcite composition. All XRPD data are presented in the supplementary materials (S4).

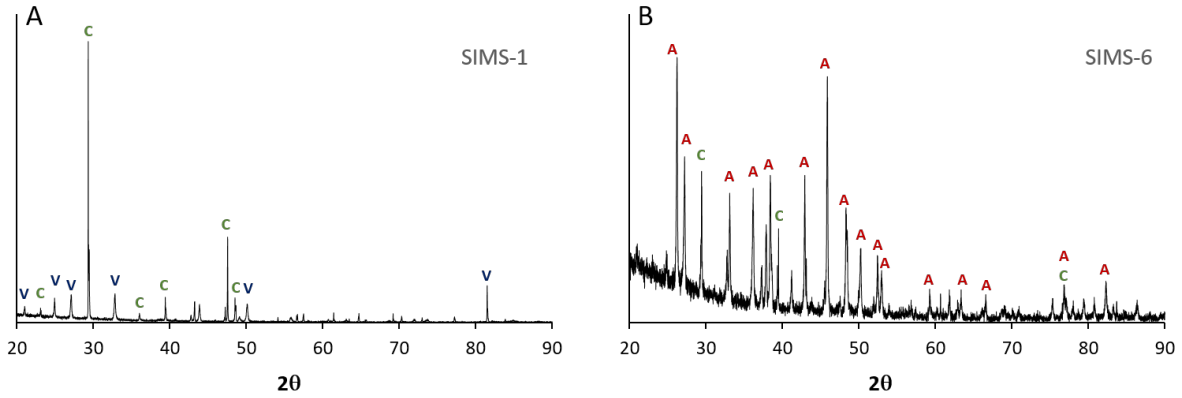

Figure 3. Example of XRPD patterns. Calcite and vaterite in experiment SIMS-1 (A); calcite and aragonite in experiment SIMS-6 (B). A, C, and V stand for aragonite, calcite, and vaterite, respectively.

Raman spectra were collected for three to five crystals of each shape—rhomboids, spherulites, and truncated pyramids. Spectra collected from rhomboids across all experiments, as well as selected truncated pyramids, display a distinct peak at 713 cm^{-1}, confirming their calcite mineralogy (Figure 4a). Another primary characteristic peak (Figure 4b) differentiates vaterite spherulites (1089–1091 cm^{-1}) from rhomboidal calcite (1087 cm^{-1}), which precipitated in experiment SIMS-1. These peak positions are consistent with the reported Raman data of Schaible et al. (2013). Additionally, a small vaterite peak at ~1075 cm^{-1} (Gauldie et al., 1997) likely contributes to a noticeable difference in peak shape. The SEM image of a vaterite spherulite is presented within Figure 4b. Raman spectroscopy also revealed that spherulites from experiments SIMS-2, 3, 6, 7, 8, and 9 exhibit a distinct peak at 706 cm^{-1}, consistent with the aragonite reference material (Figure 4c). In contrast, spherulites from experiment SIMS-4 show a distinct peak at 713 cm^{-1}, aligning with the calcite reference material (Iceland Spar). This mineralogical difference of spherulites was confirmed by higher magnification SEM imaging, where textural distinction between spherulitic calcite and aragonite was observed (Figure 4c). Also, Raman data indicate the presence of aragonite spherulites in the samples SIMS-2, 3, and 9, which were not detected by XRPD, probably due to the small amount of aragonite relative to calcite (Tables 2 and 3). Individual Raman spectra are presented in supplementary materials (S5). Due to the lack of vaterite reference material, we relied on Raman data sourced from the literature.

Table 2. Analyses of nitrogen in final experimental fluids and multiple batches of solids.

Run	Shape	XRPD mineralogy	pH	NH_4-N aq ppm	NH_4-N $CaCO_3$ ppm	NO_3-N aq ppm	NO_3-N $CaCO_3$ ppm	D(NH_4)	D(NO_3)
SIMS-1	R	n/a	8.65	1272.0	9.95	n/a	n/a	n/d	n/d
SIMS-1	mix	Cal(41), Vtr(59)	8.65	1272.0	7.56	n/a	n/a	n/d	n/d
SIMS-2	mix	n/a	8.04	1026.0	4.65	n/a	n/a	n/d	n/d
SIMS-2*	R	Cal(100)	8.04	1026.0	4.73	n/a	n/a	$4.61 \cdot 10^{-3}$	n/d
SIMS-3*	R	Cal(100)	8.08	1563.0	26.7	n/a	n/a	$17.1 \cdot 10^{-3}$	n/d
SIMS-4	mix	n/a	7.58	8220.0	86.9	n/a	n/a	n/d	n/d
SIMS-4	mix	Cal(100)	7.58	8220.0	92.3	n/a	n/a	$11.2 \cdot 10^{-3}$	n/d
SIMS-5[&]	TP	n/a	7.45	76880	190	n/a	n/a	$2.47 \cdot 10^{-3}$	n/d
SIMS-6[&]	S	n/a	7.83	6162.0	179	n/a	n/a	$29.1 \cdot 10^{-3}$	n/d
SIMS-6	mix	Arg(91), Cal(9)	7.83	6162.0	n/a	n/a	n/a	n/d	n/d
SIMS-6	R, TP	n/a	7.83	6162.0	59.4	n/a	n/a	n/d	n/d
SIMS-7[&]	S	n/a	7.85	6379.0	163	0.845	0.55	$25.6 \cdot 10^{-3}$	0.651
SIMS-7	mix	Arg(22), Cal(78)	7.85	6379.0	n/a	0.845		n/d	n/d
SIMS-7	R, TP	n/a	7.85	6379.0	48.6	0.845	0.65	n/d	n/d
SIMS-8[&]	S	n/a	7.75	6305.0	168	8.19	0.70	$26.7 \cdot 10^{-3}$	0.0855
SIMS-8	mix	Arg(35), Cal(65)	7.75	6305.0	n/a	8.19	n/a	n/d	n/d
SIMS-8	mix	n/a	7.75	6305.0	55.2	8.19	0.60	n/d	n/d
SIMS-8	R, TP	n/a	7.75	6305.0	78.8	8.19	0.90	n/d	n/d
SIMS-9[&]	S	n/a	7.92	5714.0	88.0	66.0	2.0	$15.4 \cdot 10^{-3}$	0.0296
SIMS-9*	mix	Cal(100)	7.92	5714.0	43.2	66.0	1.4	$7.56 \cdot 10^{-3}$	0.0212

Different batches of the same samples were measured in some experiments. NO_3-N and NH_4-N stand for nitrogen in nitrate and nitrogen in ammonium, respectively. Partition coefficients were calculated only for samples in which a single mineral phase was identified by XRPD, or where single mineralogy was confirmed by Raman spectroscopy on individual grains exhibiting the predominant grain morphology.

(*) - Trace quantities of aragonite spherules subsequently detected by Raman spectroscopy.
(&) - Despite the lack of XRPD data, calcite mineralogy (for R and TP) and aragonite mineralogy (for S) were confirmed by Raman spectroscopy.
Shape – crystal morphology based on visual examination of each sample batch. Cal - calcite, Vtr - vaterite, Arg – aragonite, with percentage composition provided in parentheses. n/d - not determined due to the limited sample amount; n/a - not analysed; aq- aqueous; R - rhomboids; TP – truncated pyramids; S – spherulites; mix – mixture of all grains in individual sample; n/d – not determined due to the polymineralic nature of the samples or the absence of nitrate in the system.

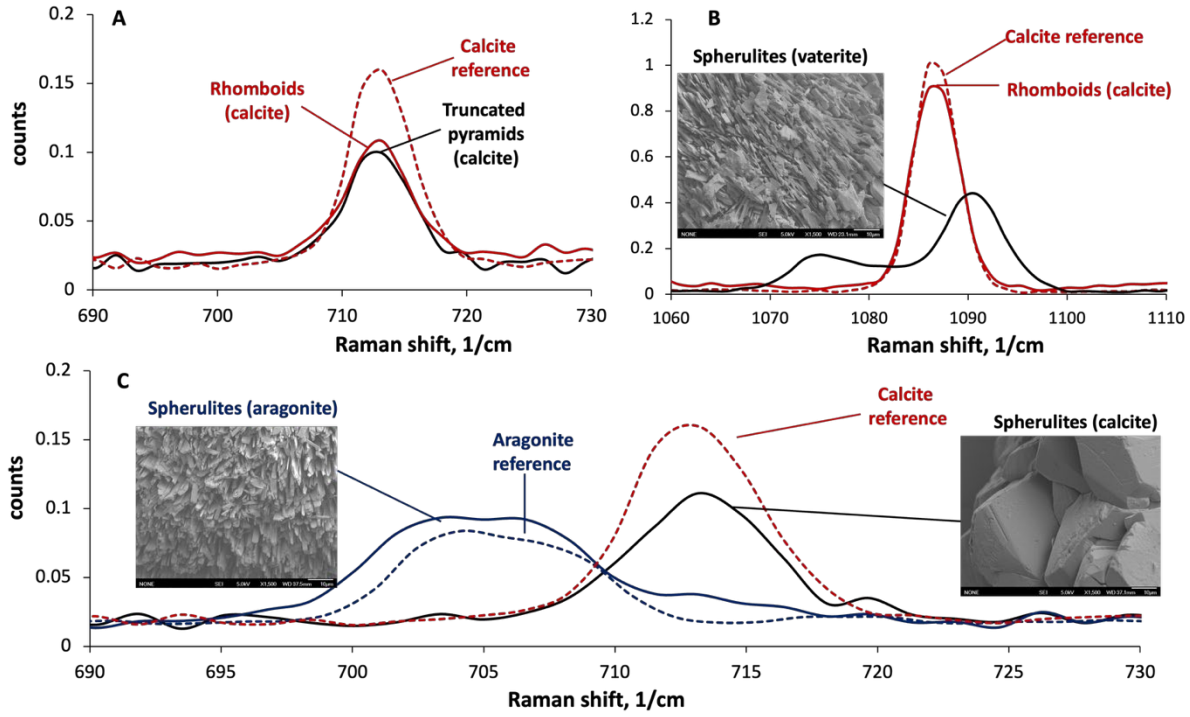

Figure 4. Average of Raman spectra of individual crystals/spherulites. A) Identification of rhomboidal and truncated pyramid calcite; B) Identification of spherulitic vaterite; C) Identification of spherulitic aragonite and calcite. Reference spectra were collected on natural Iceland Spar and aragonite monocrystals. Spherulitic textures are shown for vaterite (Fig. 4b), for aragonite and calcite (Fig. 4c).

Our data suggest that aqueous ammonium supresses the formation of vaterite and aragonite, as only calcite was observed in the experiments with high NH_4Cl concentration (SIMS-4, 5) according to both XRPD and Raman techniques. Whereas vaterite or aragonite were detected along with calcite in the experiments SIMS-1, 2, and 3, in which the growth duration (51–52 days) is similar to SIMS-4. Another key parameter in polymorph crystallization is time, as only calcite was detected in the long-term (a few months) experiment conducted by Gabitov et al. (2021) in solutions of the same NH_4Cl concentration (0.5 M) as SIMS-6, 7, 8, and 9 (42 days of duration). Therefore, aragonite and vaterite probably were intermediate mineral phases and eventually transformed into calcite in the experiment of Gabitov et al. (2021). Calcite spherulites (experiment SIMS-4) likely exhibit an intermediate texture that forms during the transformation of aragonite to calcite.

3.2 Ammonium-N and nitrate-N in post experimental carbonate crystals and fluids

The content of NH_4-N measured in large calcite rhomboids and truncated pyramids manually separated from SIMS-2–6 experiments, increases with increasing NH_4-N concentration in the experimental fluid in a non-linear manner (Figure 5A). This non-linearity is due to data from the experiment (SIMS-5), which supported the highest NH_4-N concentration in both calcite rhomboids and experimental fluids (Figure 5A). Without the inclusion of data from experiment SIMS-5, the data show a near-linear correlation (Figure 5B). These trends could be explained by the approach towards calcite saturation with NH_4 in the high-ammonium experiment (SIMS-5) or by the presence of more than one $CaCO_3$ polymorph in most of the samples, unlike SIMS-5, where only two clusters of large calcite crystals in the form of truncated pyramids precipitated.

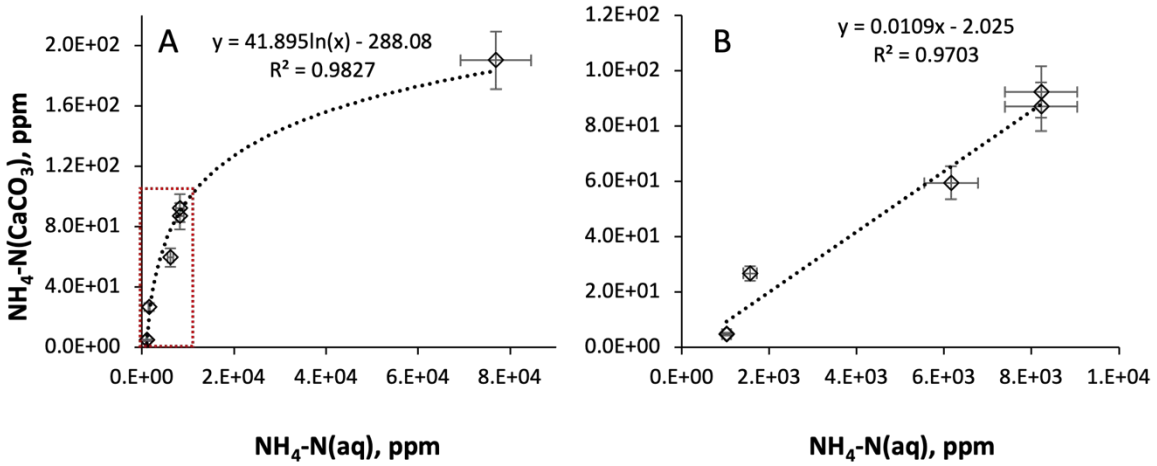

Figure 5. NH_4-N content in calcite versus its concentration in fluid for experiments SIMS-2–6 (Nitrate-free experiments). Fig. 5A includes data from experiment SIMS-5, which contained the highest ammonium concentration in both experimental fluid and product crystals. Data bounded by the red inset box are expanded in Fig. 5B, with SIMS-5 omitted.. The data from the SIMS-1 experiment are not included here as there was not enough material to conduct both AQ-2 and XRPD analyses.

In experiments (SIMS-6, 7, 8, 9), aragonite spherulites were visually separated from calcite rhomboids, and a difference in NH_4-N($CaCO_3$) content was observed between these texturally distinct crystal morphologies (Figure 6A, Table 2). In three of these experiments (SIMS-6, 7, 8), aragonite spherulites displayed NH_4-N concentrations approximately three times greater than calcite rhomboids. This difference between aragonite and calcite is approximately two times smaller in experiment SIMS-9. Analyses of individual grains via SIMS, which eliminated any morphological cross-contamination effect from visually separating polymorphs, are presented below in section 3.3.

The content of NO_3-N measured in fluid and $CaCO_3$ samples from nitrate-doped experiments (SIMS-7, 8, 9) is presented in Figure 6B and Table 2. The concentration of NO_3-N in $CaCO_3$ increases with concentration in the fluid. There, the linear fit of data obtained fromspherulites is steeper than that obtained from rhomboids. Unlike ammonium, no systematic difference in nitrate content was observed while comparing rhomboids and spherulites.

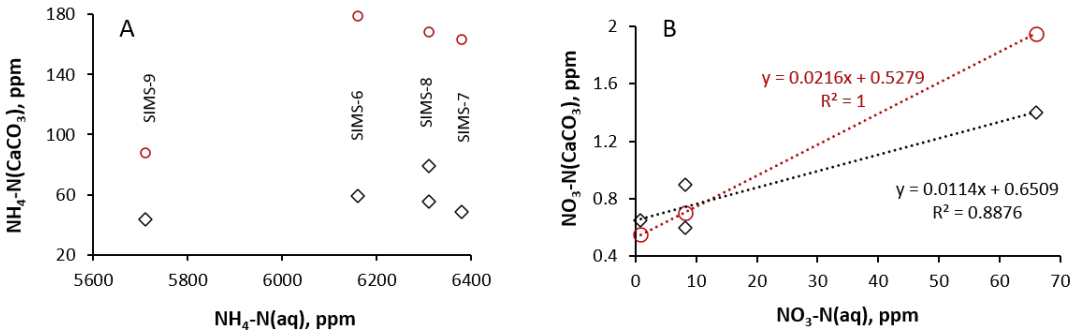

Figure 6. Nitrogen content (analysed by AQ2) in rhomboids (diamonds) and spherulites (circles) versus its concentration in fluid with initial ammonium of 0.5 M and variable nitrate concentration: A) Ammonium; B) Nitrate for the samples SIMS-7,8,9.

3.3 Ion microprobe analyses of total nitrogen in individual grains of $CaCO_3$

Optical microscopy images in Figures 7 and 8 show polished calcite, vaterite, and aragonite grains embedded in epoxy. During each ion microprobe spot analysis, a small area of $CaCO_3$ was destroyed with the ion beam, leaving a rectangular mark with a dimension of 40 µm * 30 µm (Figure 7a, b). Up to four grains of calcium carbonate from each experiment were examined by ion microprobe, and the average values for each grain (n=2 to n=17) are presented in Table 3. The data confirmed that aragonite and vaterite spherulites are always enriched in total nitrogen compared to calcite rhomboids for each individual experiment. The only exception to this pattern of spherulites being enriched compared to rhomboids was observed in experiment SIMS-4 (supplementary materials S3 and S6). There the average CN/CC values for SIMS-4 calcite spherulites and rhomboids overlap within 1 s.e. (standard deviation divided by the square-root of n), i.e., CN/CC(rhomboids)=0.892±0.508 and 0.655±0.635 whereas CN/CC(spherulites)=1.17±0.129 cps/cps, which is not the case for other experiments, where spherulites consist of aragonite and vaterite (Table 3).

An assessment of intra-crystalline heterogeneity was undertaken, with the aim of producing a carbonate reference material that could be used for ion microprobe calibration. Ion microprobe data show that individual calcite crystals (rhomboids and truncated pyramids) are highly heterogeneous in nitrogen (1 s.e.>50%), with some data points being up to an order of magnitude different from adjacent locations (e.g., Figure 7b). The large errors associated with averaged data points (1.s.e. of the multiple analytical spots) are presented in Table 3. Given the high heterogeneity of the SIMS CN/CC data, the measurements were separated into two groups, referred to as high-N and low-N calcite. The criterion for identifying high-N calcite was a difference of at least one order of magnitude between the low-N and high-N populations, except for experiments SIMS-1 and SIMS-2, where a minimum difference of a factor of two was applied. The biggest synthesized crystal (SIMS-5) yielded the largest dataset (17 spots) with all labelled on the photomicrograph (Figure 8). Although no spatial control on nitrogen content in this crystal was observed, the difference in nitrogen concentration between high-N and low-N groups is almost two orders of magnitude. Figure 8 shows the nitrogen content in each group, calculated from both the ammonium concentrations in bulk calcite (AQ-2 analyses) and CN/CC ratios (SIMS analyses) using equation 1 and 2:

$$(\mathrm{N})_{high-N} = (\mathrm{NH_4 - N})_{AQ-2} \cdot (\mathrm{CN/CC})_{\mathrm{high-N}} / (\mathrm{CN/CC})_{\mathrm{all\ data}} \quad \text{[Eq. 1]}$$

$$(\mathrm{N})_{low-N} = (\mathrm{NH_4 - N})_{AQ-2} \cdot (\mathrm{CN/CC})_{\mathrm{low-N}} / (\mathrm{CN/CC})_{\mathrm{all\ data}} \quad \text{[Eq. 2]}$$

Where CN/CC are the averages of SIMS data from high-N and low-N groups as well as the average of all SIMS data collected on this individual crystal.

398

399 **Table 3.** Ion microprobe data from the two analytical sessions: average of each $CaCO_3$ grain.

Experiment	Raman Mineralogy / crystal shape	Grain no.	n	CN/CC cps/cps	1.s.e	NH_4-N $CaCO_3$ ppm	NO_3-N $CaCO_3$ ppm
Session-1: Comparison of rhomboids, truncated pyramids, and spherulites							
SIMS-1	Cal / R	1	2	0.0758	0.0145	7.53	n/a
SIMS-1	Cal / R	2	2	0.0676	0.00207	7.53	n/a
SIMS-2	Cal / R	1	3	0.0275	0.0133	4.73	n/a
SIMS-3	Cal / R	1	3	0.249	0.121	26.7	n/a
SIMS-4	Cal / R	1	3	**0.655**	0.635	**92.3**	n/a
SIMS-6	Cal / TP	1	3	0.683	0.502	59.4	n/a
SIMS-7	Cal / TP	1	3	0.405	0.0115	48.6*	0.65*
SIMS-8	Cal / TP	1	3	1.41	0.411	55.2*	0.90*
SIMS-9	Cal / R	1	3	0.176	0.173	43.2	1.4[&]
SIMS-1	Vtr / S	1	2	0.394	0.0195	7.53	n/a
SIMS-1	Vtr / S	2	2	0.215	0.00440	7.53	n/a
SIMS-2	Arg / S	1	3	0.759	0.0190	4.73	n/a
SIMS-3	Arg / S	1	3	1.82	0.0770	26.7	n/a
SIMS-3	Arg / S	2	3	1.75	0.0638	26.7	n/a
SIMS-4	Cal / S	1	3	1.17	0.129	92.3	n/a
SIMS-6	Arg / S	1	3	3.50	0.0444	179	n/a
SIMS-6	Arg / S	2	3	3.33	0.141	179	n/a
SIMS-7	Arg / S	1	8	3.46	0.0484	163	0.55
SIMS-7	Arg / S	2	4	2.83	0.0478	163	0.55
SIMS-8	Arg / S	1	7	3.36	0.0220	168	0.70
SIMS-9	Arg / S	1	3	2.71	0.212	88.0	2.0
SIMS-9	Arg / S	2	3	2.75	0.116	88.0	2.0
Session-2: Heterogeneity of individual calcite crystals							
SIMS-1	Cal / R	3	3	0.0507	0.0321	7.53	n/a
SIMS-2	Cal / R	3	4	0.0235	0.0149	4.73	n/a
SIMS-3	Cal / R	3	4	0.287	0.0958	26.7	n/a
SIMS-4	Cal / R	3	4	0.892	0.508	92.3	n/a
SIMS-5	Cal / TP	1	17	2.39	0.502	190	n/a
SIMS-6	Cal / R	3	4	0.886	0.0577	59.4	n/a
SIMS-6	Cal / TP	4	3	0.0857	0.0521	59.4	n/a

All grains were collected from the walls of the growth containers. Cps = counts per second. n represents the number of analytical spots collected at various locations that comprise the average cps data for an individual crystal or spherulite. CN/CC is an average of the intensity ratios $^{12}C^{14}N/^{12}C^{12}C$ (cps/cps), which are presented in the Table S-6. Cal, Vtr, and Arg are calcite, vaterite, and aragonite. R, S, and TP are rhomboids, spherulites, and truncated pyramids. NH_4-N($CaCO_3$) was determined by AQ-2. 1 s.e. = standard deviation / $\sqrt{n}$

(*) – ammonium and nitrate data are from AQ-2 analyses of the mixtures of R and TP.

([&]) – ammonium and nitrate data are from AQ-2 analyses of the mixtures of all shapes in SIMS-9, where only calcite was detected with XRPD.

400

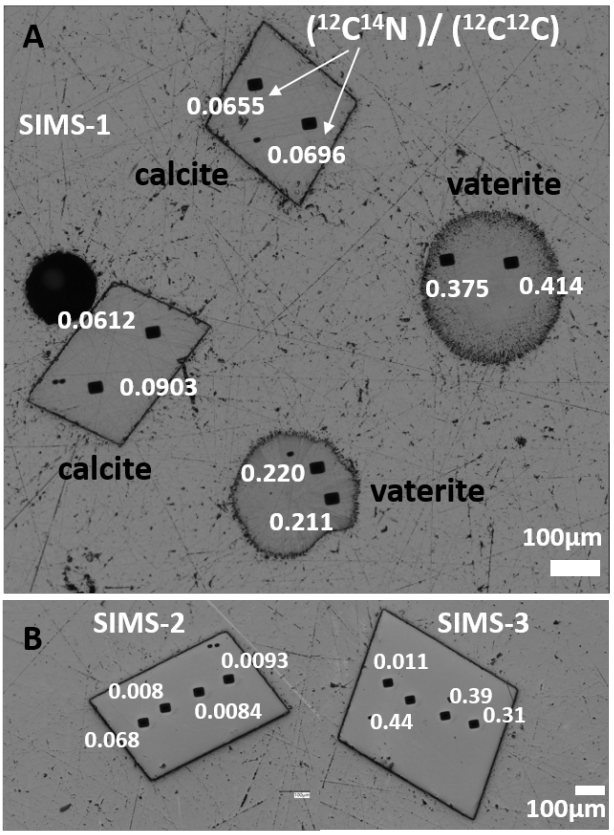

Figure 7. Examples of SIMS intensity ratios collected on rhomboids and spherulites. Fig. 7A An example of the location of ion beam spot analyses on the polished $CaCO_3$ of the sample SIMS-1; numbers correspond to CN/CC. Fig 7B An example of the location of ion beam spot analyses on the polished calcite crystals of the samples SIMS-2 and SIMS-3.

Spherulites resulted in a polycrystalline phase which was more homogeneous in nitrogen at the applied spatial resolution (Figure 8). The 1 s.e. values for aragonite and vaterite spherulites are much smaller than those for calcite rhomboids and generally do not exceed 10%. This is likely due to the relatively large size of the ion microprobe analytical spots, which exceed the thickness of individual spherulite needles (< 10 µm) and therefore yield an average nitrogen content from an area of 40 µm * 30 µm. Therefore, potential sectoral zoning (as inferred to exist in rhomboids) was not detectable in the spherulites. This leads to lower standard errors within individual aragonite or vaterite spherulites compared to calcite rhomboids (Table 3). The smallest intra-spherulite variability in nitrogen (1 s.d.=1.7-4.0 % or 1 s.e.=0.65-1.4 %) was achieved when the number of analytical spots (n) exceeded 3. At n=3, 1 s.d. was as high as 13.5 % or even 19 % in the texturally distinct calcite spherulite from experiment SIMS-4, which is the only experiment where spherulites have calcite mineralogy. This observation is consistent with the different microtextures observed in the spherulites: calcite spherulites from SIMS-4 consist of equant, semi-transparent crystals, whereas aragonite (SIMS-2) and vaterite (SIMS-1) spherulites are composed of needle-like crystals radiating from the center (Figure 2). The equant calcite crystals within the SIMS-4 spherulites likely contain sectoral zonation, which increases intra-spherulite heterogeneity to as much as 19%.

The largest datasets (n=8 and n=7) of two individual aragonite spherulites from experiments SIMS-7 and 8, where the initial ammonium concentration in the growth media was the same, are shown in Figure 8. An order of magnitude difference in the initial aqueous nitrate concentration (1 and 10 ppm) did not affect the ion microprobe data, as averaged CN/CC

are very similar in these samples (3.5 and 3.4 cps/cps for SIMS-7 and SIMS-8 spherulites), with standard deviations of 4.0 and 1.7 % respectively. This suggests larger spherulites grown in a solution of 0.5 M NH_4Cl and 0.01 M $CaCl_2$ by the CO_2 diffusion technique have the potential to be used as ion microprobe reference materials for nitrogen, and possibly its isotopes. This method should enable spatial resolution of analysis at 30 µm, with N=164-169 ppm and at a precision of <10% (1.s.d.), where the N-range is the range of total nitrogen in aragonite spherulites of the samples SIMS-7 and 8. The inter-spherulite variability was calculated between pairs of spherulites in five experiments (Table 3). There, the largest 1 s.d. of 41 % (1 s.e. of 29%) was observed between small vaterite spherulites 1 and 2 from experiment SIMS-1. In the other four experiments (SIMS-3, 6, 7, and 9), inter-spherulite variability in larger spherulites varied from 1.0 to 14 % of 1 s.d. (1 s.e.=0.73–10%) with the average 1 s.d. value of 5.4 % (or average 1 s.e.=3.8%).

Table 4. Selected data (high-N) of nitrogen in nitrate-free calcites.

Experiment	CN/CC	1s.d.	n	1s.e.	NH_4-N, ppm	log(CN/CC)	1s.e.	log(NH_4-N)
SIMS-1	0.0801	0.0219	5	0.00980	7.56	-1.10	0.0566	0.876
SIMS-2	0.0499	0.0158	3	0.00910	4.73	-1.30	0.0877	0.675
SIMS-3	0.375	0.0509	5	0.0228	26.7	-0.426	0.0272	1.43
SIMS-4	1.82	0.0905	3	0.0522	92.3	0.261	0.0126	1.96
SIMS-5	3.53	0.797	12	0.278	190	0.526	0.0375	2.28
SIMS-6	1.04	0.367	5	0.164	59.4	0.0185	0.0743	1.77

NH_4-N data are from AQ-2 analyses of calcite bulk. The criterion for selecting high-N calcite was a difference of at least one order of magnitude between low-N and high-N calcite, except for experiments SIMS-1 and SIMS-2, where a minimum difference of a factor of two was used.

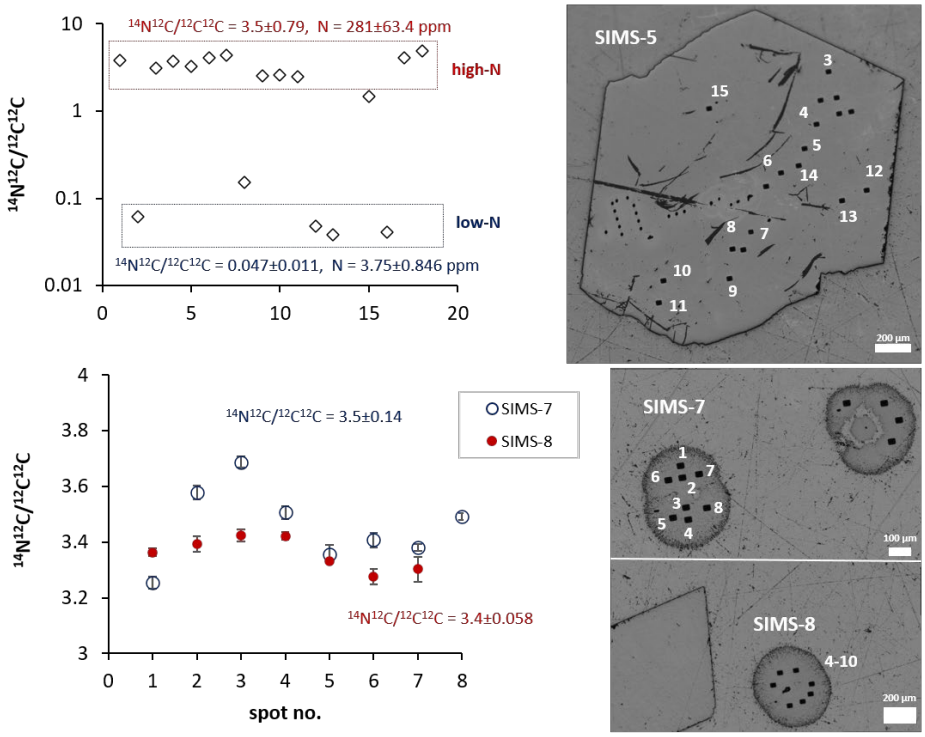

Figure 8. An assessment of intra-crystalline heterogeneity of the largest rhomboid (experiment SIMS-5) and spherulites (experiments SIMS-7 and 8) with photomicrographs.

Average CN/CC ratios and calculated N concentrations for high-N and low-N groups are presented on the plots.

Notwithstanding the heterogeneity of intra- and inter-crystalline N concentrations, as measured by ion microprobe and defined above, plots of averaged ion probe CN/CC versus bulk AQ2-N show potential for use as a SIMS calibration data set. Plots of CN/CC intensity ratios versus AQ-2 ammonia content of calcite are presented in Figure 9 for: a) All ion microprobe data collected from crystal morphologies grown as a part of experiments SIMS-1–6 (1 s.e. within individual growth experiments ranges between 21.0 to 63.5 %); b) High-N SIMS data, where low-N spots were excluded (1 s.e. within individual growth experiments with low-N data removed ranges between 2.87 to 15.7 %) (see also Table 3 and Table 4). Data from samples SIMS-7, SIMS-8, and SIMS-9 are not included in the plot, as these samples were mounted separately and analysed in different ion microprobe analytical sessions, potentially introducing offsets due to the absence of a nitrogen reference. The R^2 values for calibration curves obtained from both data sets are above 0.99. Based on the calibration curves presented in Figure 9, we thus consider the use of multiple carbonate crystals grown according to the CO_2 diffusion protocol presented here, may be considered appropriate as SIMS calibration materials for nitrogen at concentrations ranging between 7.53 and 190 ppm.

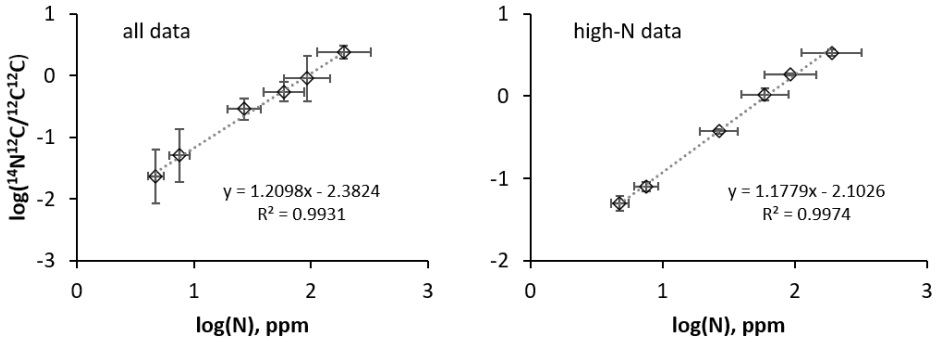

Figure 9. Calibration curves of ion microprobe CN/CC (cps/cps) and AQ-2 nitrogen (ppm) data. Ion probe data collected on calcites from experiments SIMS-1–6 are from an individual session-2 (Table 3), data are the averages from each experiment.

4. Discussion

4.1 Partitioning of ammonium and nitrate between $CaCO_3$ polymorphs and aqueous growth media

To evaluate a relationship between nitrogen contained in the aqueous growth media and N-bearing polymorphs of $CaCO_3$ (measured with AQ-2), Nernst partition coefficients (D) were calculated for ammonium as $D(NH_4) = NH_4\text{-}N(CaCO_3) / NH_4\text{-}N(aq)$ and for nitrate as $D(NO_3) = NO_3\text{-}N(CaCO_3) / NO_3\text{-}N(aq)$. In experiments SIMS 4 and 5, and in the selected calcite batches from experiments SIMS 2 and 3, $D(NH_4)$ values were calculated to range from $2.47 \cdot 10^{-3}$ to $17.1 \cdot 10^{-3}$ (Table 2). We were able to manually separate spherulites, which were predominantly of aragonite mineralogy, from bulk crystals and run AQ-2 analyses in four samples (SIMS-6, 7, 8, and 9), where the mass of extracted crystals was sufficiently high. Partition coefficients for incorporation of ammonium into aragonite spherules range between $15.4 \cdot 10^{-3}$ and $29.1 \cdot 10^{-3}$ (Table 2). This suggests that ammonium is more compatible with aragonite than with calcite. This difference in ammonium compatibility between calcite and aragonite is corroborated by sample SIMS-9. In the sample SIMS-9mix, where only calcite was identified by XRPD, AQ-2 analyses revealed a low partition coefficient for ammonium

($D(NH_4) = 7.56 \cdot 10^{-3}$; Table 2). In contrast, analyses of coexisting spherulites from the same experiment (SIMS-9S) revealed higher ammonium concentrations, corresponding to a higher partition coefficient ($D(NH_4) = 15.4 \cdot 10^{-3}$). Nitrate D values in SIMS-9mix, which were identified as calcite with XRPD, is 0.0212 (Table 2). Nitrate D values in aragonite spherulites (SIMS-9S), which were identified as aragonite with Raman spectroscopy, is 0.0296.

Ion microprobe analyses of individual grains showed that calcium carbonate polymorph-controlled uptake is even stronger than observed with AQ-2 bulk ammonium analyses, such that aragonite and vaterite spherulites were found to be enriched with respect to calcite rhomboids by up to a factor of 15, as shown for the sample SIMS-9 (Table 3). No physical separation of polymorphs was performed prior to AQ2 analyses in sample SIMS-1, i.e., AQ-2 and XRPD data represent the mixture of both morphologies. Therefore, in this sample, mass balance calculations were performed using SIMS intensity ratios and AQ2 concentration data to evaluate ammonium partition coefficients in polymorphs, where vaterite and calcite yielded abundances of 59 % and 41 % respectively (Table 2).

$$\mathrm{N-NH_4(Vtr)} = (\mathrm{CN/CC})_{\mathrm{Vtr}} / (\mathrm{CN/CC})_{\mathrm{Mix}} \cdot \mathrm{N}_{\mathrm{MIX}}^{\mathrm{AQ-2}} \quad \text{[Eq. 3]}$$

$$\mathrm{N-NH_4(Cal)} = (\mathrm{CN/CC})_{\mathrm{Cal}} / (\mathrm{CN/CC})_{\mathrm{Mix}} \cdot \mathrm{N}_{\mathrm{Mix}}^{\mathrm{AQ-2}} \quad \text{[Eq. 4]}$$

Here $\mathrm{N_{Vtr}}$ and $\mathrm{N_{Cal}}$ are nitrogen content in vaterite and calcite; CN/CC is an average of intensity ratios (cps/cps) from ion microprobe analyses for vaterite $(\mathrm{CN/CC})_{\mathrm{Vtr}} = 0.3045$, calcite $(\mathrm{CN/CC})_{\mathrm{Cal}} = 0.06270$ and their mixtures:

$$(\mathrm{CN/CC})_{\mathrm{Mix}} = (\mathrm{CN/CC})_{\mathrm{Vtr}} \cdot 0.59 + (\mathrm{CN/CC})_{\mathrm{Cal}} \cdot 0.41 = 0.2054 \quad \text{[Eq. 5]}$$

$\mathrm{N}_{\mathrm{MIX}}^{\mathrm{AQ-2}}$ is NH_4-N measured by AQ-2 (7.525 ppm).

$$\mathrm{D}_{\mathrm{Vtr}}^{\mathrm{NH4}} = \mathrm{N-NH_4(Vtr)} / \mathrm{N_{Fluid}} = 11.16 / 1272 = 8.77 \cdot 10^{-3}; \quad \text{[Eq. 6]}$$

$$\mathrm{D}_{\mathrm{Cal}}^{\mathrm{NH4}} = \mathrm{N-NH_4(Cal)} / \mathrm{N_{Fluid}} = 2.297 / 1272 = 1.81 \cdot 10^{-3}. \quad \text{[Eq. 7]}$$

Similar calculations were performed for aragonite spherulites and calcite rhomboids from experiments SIMS-6, 7, and 8 (Table 5). Here, XRPD yielded both mineral phases and partition coefficients for specific polymorphs calculated by ion microprobe mass balance could be compared directly to those quantified by AQ2 analysis. The calculated partition coefficients are summarized in Table 5, where $D(NH_4)$ values are higher for aragonite and vaterite compared to co-existing calcite. This ion microprobe-based difference is more pronounced for aragonite and calcite in samples SIMS-6 and 7 compared to AQ-2 data on visually separated spherulites from bulk crystal mixes shown in Table 2. Additionally, the ion microprobe-derived values of $\mathrm{D}_{\mathrm{AR}}^{\mathrm{NH4}}$ (Table 5) are comparable to, or approximately half of, the AQ-2-based values (Table 2). This discrepancy is likely due to variations in the calcite-to-aragonite ratio among different sample batches. Note that experiments SIMS 7 and 8 contained nitrate at ppm levels and an order of magnitude concentration difference in the aqueous growth media (1 and 10 ppm. respectively). However, these nitrate concentrations in the growth media had an insignificant effect on the SIMS data, as CN/CC values are very similar in these samples (3.5 and 3.4 cps/cps for SIMS-7 and SIMS-8 spherulites), with standard deviations of 4.0 and 1.7 % respectively. Nitrate in the aqueous growth media thus generated no difference in $D(NH_4)$, which was well below the analytical error and the variability due to nitrogen heterogeneity. Overall, the average $\mathrm{D}_{\mathrm{AR}}^{\mathrm{NH4}}$ of 0.0163 is five times higher than average $\mathrm{D}_{\mathrm{CAL}}^{\mathrm{NH4}}$ of 0.00309 (Table 5).

Although the clear difference in ammonium uptake between calcite and other polymorphs was identified via two different techniques at the macro (AQ-2) and ion microprobe scales,

there is a potential caveat in the interpretation of these data due to textural difference. Unlike calcite rhomboids, vaterite and aragonite spherulites can contain ammonium between needle-like crystals at the sub-µm scale, which could cause an overestimation of the analysed NH_4-N. Such an effect was not observed for nitrate uptake as its concentration in the fluid is much lower than the ammonium concentration. However, this hypothesis—that ammonium is entrapped at the surface of individual microcrystals—was not corroborated by ion microprobe analyses of the sample SIMS-4, as the CN/CC values of calcite spherulites overlap with those of rhomboids, suggesting the preferential incorporation of ammonium into aragonite spherules was controlled by carbonate polymorph rather than crystal morphology.

Unlike ammonium uptake, nitrate uptake by $CaCO_3$ does not systematically depend on polymorph or crystal morphology, suggesting that there is no difference between partition coefficients ($D(NO_3)$) for aragonite and calcite. Therefore, $D(NO_3)$ values of unseparated $CaCO_3$ mixtures are similar to those of spherulites picked from a pile of mixed crystals (Table 2 and Figure 10). The $D(NO_3)$ decreases from 0.769 to 0.021 when NO_3(aq) in the growth media increases from 0.84 to 66.0 ppm. These experimentally determined values are about 2 times lower than $D(NO_3)$ re-calculated from speleothem nitrate data in Wynn et al. 2021 (0.48–2.6, average of 1.3). Despite a drastic difference in the composition of the aqueous growth media, i.e., high ammonia chloride in our experimental system, in contrast with low salinity drip waters in the cave system (Wynn et al. 2021), both datasets show similar trends. This suggests that nitrate uptake occurred out of equilibrium, which is common for ion incorporation to calcite under environmental conditions. For sulphate uptake into the carbonate crystal lattice, pH and crystal growth rate were demonstrated to be key controlling factors (Wynn et al. 2018). However, for nitrate, neither pH nor growth rate can explain the trend observed in our experiments (Figure 10). Growth media composition (NH_4Cl and $CaCl_2$) and thus pH were similar in SIMS-7, 8, and 9 (Tables 1 and 2). The concentration of aqueous nitrate is the only difference (x100) between the experiments, suggesting competition of NO_3^- with CO_3^{2-} during uptake into the carbonate lattice and/or modification to the carbonate surface (Hofmann 2016) may have affected the crystallization reaction and nitrate uptake.

Table 5. Calculated ammonium partition coefficients for vaterite, aragonite, and calcite ($D^{NH4}_{Vtr,Arg,Cal}$).

	SIMS-1	SIMS-6	SIMS-7	SIMS-8
XRPD: Vtr %	59	n/a	n/a	n/a
XRPD: Arg %	n/a	91	22	35
XRPD: Cal %	41	9	78	65
$(CN/CC)_{Vtr}$	0.3045	n/a	n/a	n/a
$(CN/CC)_{Arg}$	n/a	3.415	3.458	3.358
$(CN/CC)_{Cal}$	0.06270	0.5850	0.4050	1.410
$(CN/CC)_{Mix}$	0.2054	3.160	1.077	2.092
$N-NH_4(Vtr)$, ppm	11.16	n/a	n/a	n/a
$N-NH_4(Arg)$, ppm	n/a	64.18	156.1	88.55
$N-NH_4(Cal)$, ppm	2.297	10.99	18.29	37.18
D^{NH4}_{Vtr}	$8.77\cdot10^{-3}$	n/a	n/a	n/a
D^{NH4}_{Arg}	n/a	$10.4\cdot10^{-3}$	$24.5\cdot10^{-3}$	$14.0\cdot10^{-3}$
D^{NH4}_{Cal}	$1.81\cdot10^{-3}$	$1.78\cdot10^{-3}$	$2.87\cdot10^{-3}$	$5.90\cdot10^{-3}$

Data are based on AQ-2 and ion microprobe analyses. Vtr, Arg, Cal, and Mix are vaterite, aragonite, calcite, and a mixture of two $CaCO_3$ minerals, respectively, i.e., Cal+Vtr or Cal+Arg. $(CN/CC)_{Vtr,\ Arg,\ Cal}$ averages ion microprobe intensity ratios of $^{12}C^{14}N/^{12}C^{12}C$ of multiple spots in vaterite, aragonite, and calcite, respectively, i.e., the weighted average of the CN/CC data presented in Table 3. $(CN/CC)_{MIX}$ was calculate using equation 5. Concentrations of ammonium nitrogen, i.e., $N-NH_4(Vtr,\ Cal)$, were calculated using equations 3 and 4 for vaterite and calcite (similarly for aragonite). Partition coefficients $D_{Vtr,CAL}^{NH4}$ were calculated using equations 6 and 5 for vaterite and calcite (similarly for aragonite).

The high intra-crystalline heterogeneity observed in the calcites is consistent with previous studies on other elements distribution in similarly grown calcite. Sectoral zoning of boron (B) in calcite was reported by Hemming et al. (1998), and partition coefficients of B and lithium (Li) between calcite sectors and growth media were evaluated by Gabitov et al. (2021). The growth entrapment model (Watson et al. 2004) provides a possible explanation for this heterogeneity, where observed sectoral zoning occurred because of the differences in surface enrichment factors of geometrically non-equivalent adjacent sectors. The nature of contrasting surface enrichment factors was suggested by Hemming et al. (1998) to be due to different rates of adsorption of tetragonal boron species and their conversion to trigonal species (BO_3^-), which are abundant in calcite. A more significant uptake of B by vicinal faces with acute growth steps compared to those with obtuse growth steps was ultimately suggested to cause the observed sectoral zoning.

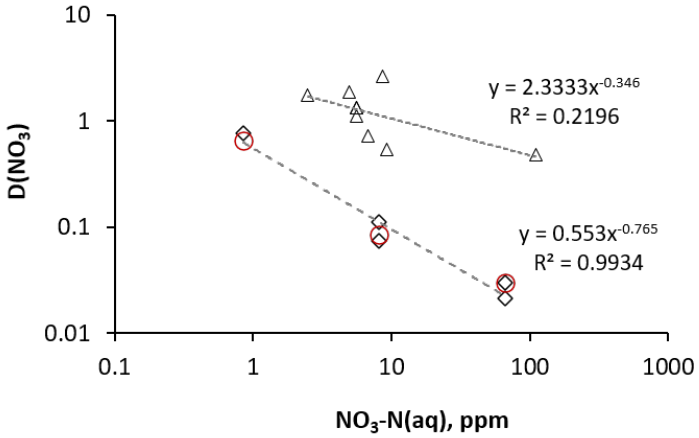

Figure 10. Nitrate uptake by experimental $CaCO_3$ and speleothem calcite (triangles, Wynn et al. 2021). Diamonds are unseparated mixtures of calcite and aragonite analysed with AQ-2; circles are picked spherulites (aragonite in SIMS-7, 8 and calcite in SIMS-9).

Overall, the carbonate textures produced in this study are relevant to natural settings. Aragonite and vaterite spherulites resemble many biogenic marine and freshwater minerals, such as corals and fish otoliths (Dauphin, 2001; Mukkamala et al., 2006; Weiner and Addadi, 2011; Christy, 2017). Corals benefit from spherulitic growth because aragonite crystals grow up to 10 times faster along the c-axis than the a-axis. In spherulites, where growth is primarily along the fast c-axis, this geometry allows for more efficient space filling than any other growth pattern (Sun et al. 2017). Similarly, calcite and aragonite spherulites can be texturally analogous to speleothems found in terrestrial and coastal caves (Fairchild et al., 2006; Frisa, 2015). Therefore, the obtained partitioning data could be applied as a proxy for carbonate deposits to study ammonia and nitrate cycling.

5. Conclusions

Understanding the role of nitrogen in the carbonate palaeorecord depends upon quantitative knowledge of partitioning across the aqueous - $CaCO_3$ interface. Partitioning is seen to vary depending on nitrogen species and carbonate polymorph. Ammonium demonstrated a greater efficiency of incorporation into synthesised crystals of aragonite and vaterite compared to calcite. Ion microprobe analysis revealed a more homogenous distribution of ammonium within the aragonite and vaterite spherulites, as opposed to within calcite rhomboids. Individual large aragonite spherulites are homogeneous in nitrogen within 10% of the relative standard deviation. Calcite rhomboids were monocrystalline, with heterogeneity likely arising due to sectoral zoning. However, aragonite and vaterite spherulites were polycrystalline. An analytical spot size larger than the width of individual spherulite needles thereby masked any potential heterogeneity between these crystalline needles. Nitrate partitioning into $CaCO_3$ demonstrated a higher compatibility with all polymorphs, with no distinction in partition coefficients between calcite and aragonite phases. A combination of bulk automated colourimetry (AQ-2, providing absolute concentrations of N in calcium carbonate) and ion microprobe techniques (providing count rates of CN/CC at the μm scale) suggests that calcium carbonate polymorphs, grown by the adopted protocol where ammonium is a predominant nitrogen aqueous species, have a potential to be used as reference materials for the development of a nitrogen calibration curve. This represents an initial step toward developing a carbonate nitrogen standard, as substantial intracrystalline heterogeneity was observed within individual calcite crystals. By improving our understanding of how nitrogen species may be incorporated into carbonate polymorphs, and by developing preliminary reference materials for calibrating micro-analytical techniques, this study provides a foundation for exploring the potential role of nitrogen in the carbonate palaeorecord.

6. Acknowledgements

This study was supported by the Fulbright-Lancaster University (STEM-Science and Technology) Scholar Award (#10331-UK) and by the Global Development Seed Grant awarded by the International Institute at Mississippi State University (MSU). The pilot ion microprobe analyses were supported by the UK NERC Ion Microprobe Facility at The University of Edinburgh. We thank: The Departments of Geosciences, Physics, and Astronomy at MSU; Lancaster Environment Centre and Department of Chemistry at Lancaster University; and The Ion Microprobe Laboratory at UCLA, which is partially funded by grant EAR-2154590 from NSF's Instrumentation and Facilities Program. We thank Drs. Hailiang Dong (Executive Editor) and Abby Ren (Associate Editor) for handling the manuscript and two anonymous reviewers for their helpful comments and suggestions.

7. Data Availability

Data are available through Mendeley Data at DOI:10.17632/3c5ym3gwn2.3

8. Appendix A. Supplementary Material

S1_Edinburgh ims-7f-geo: Data collected at the NERC Ion Micro-Probe (SIMS) Facility, University of Edinburgh, using the CAMECA IMS 7f-GEO instrument. The $^{12}C^{14}N$ counts per second were calculated by correcting the total intensity at 26 amu for $^{13}C^{13}C$ interference (see main text for details).

S2 Micrograph of SIMS 1-5 mounted crystals coated with gold: Optical micrograph of mounted and polished calcite crystals (SIMS-1 to SIMS-6) prepared for ion microprobe analysis. The inset images of individual crystals show the SIMS analytical spot sites. Numbered analytical spots represent analysis undertaken using the CAMECA IMS 1290 instrument at UCLA, summarized in Tables 3 and 4 in the main manuscript text.

S3 Micrograph of SIMS-6–9 mounted crystals coated with gold: Optical micrograph of mounted and polished rhomboids and spherulites (SIMS-1–4, SIMS-6–9) prepared for ion microprobe analysis. The inset images of individual crystals show the SIMS analytical spot sites. Numbered analytical spots represent analysis undertaken using the CAMECA IMS 1290 instrument at UCLA, summarized in Tables 3 and 4 in the main manuscript text.

S4 XRPD: X-ray powdered diffraction results for crystal products from each experiment (SIMS-1–9).

S5 Raman: Raman spectroscopy data for crystal products from each experiment (SIMS-1–9), including spectra for reference materials and different morphological types.

S6 UCLA SIMS CAMECA IMS-1290: Data collected at the UCLA SIMS Laboratory using the CAMECA IMS 1290 instrument. Each mount is presented on a separate sheet.

9. References

Andersson, R.A., Meyers, P., Hornibrook, E., Kuhry, P. and Mörth, C.M., 2012. Elemental and isotopic carbon and nitrogen records of organic matter accumulation in a Holocene permafrost peat sequence in the East European Russian Arctic. *Journal of Quaternary Science*, 27(6), 545–552.

Christy, A.G., 2017. A review of the structures of vaterite: the impossible, the possible, and the likely. Crystal Growth & Design, 17(6), 3567–3578.

Dauphin, Y., 2001. Comparative studies of skeletal soluble matrices from some Scleractinian corals and Molluscs. International Journal of Biological Macromolecules, 28(4), 293–304.

Dean, J. R., Leng, M. J., & Mackay, A. W. (2014). Is there an isotopic signature of the Anthropocene? *The Anthropocene Review*, *1*(3), 276–287. https://doi.org/10.1177/2053019614541631

Fairchild, I.J., Smith, C.L., Baker, A., Fuller, L., Spötl, C., Mattey, D. and McDermott, F., 2006. Modification and preservation of environmental signals in speleothems. Earth-Science Reviews, 75(1-4), 105–153.

Frisia, Silvia. 2015. Microstratigraphic logging of calcite fabrics in speleothems as tool for palaeoclimate studies. International Journal of Speleology, 44: 1–16.

Gabitov, R.I., Sadekov, A. and Leinweber, A., 2014. Crystal growth rate effect on Mg/Ca and Sr/Ca partitioning between calcite and fluid: An *in-situ* approach. Chemical Geology, 367, 70–82.

Gabitov, R.I., Sadekov, A., Dyer, J., Perez-Huerta, A., Xu, H. and Migdisov, A., 2021. Sectoral and growth rate control on elemental uptake by individual calcite crystals. Chemical Geology, 585, p.120589.

Galloway, J.N., Townsend, A.R., Erisman, J.W., Bekunda, M., Cai, Z.C., Freney, J.R., Martinelli, L.A., Seitzinger, S.P., Sutton, M.A., 2008. Transformation of the nitrogen cycle: recent trends, questions, and potential solutions. Science 320, 889–892.

Gauldie, R.W., Sharma, S.K. and Volk, E., 1997. Micro-Raman spectral study of vaterite and aragonite otoliths of the coho salmon, Oncorhynchus kisutch. *Comparative Biochemistry and Physiology Part A: Physiology*, *118*(3), 753–757.

Glock, N., Liebetrau, V., Vogts, A. and Eisenhauer, A., 2019. Organic heterogeneities in foraminiferal calcite traced through the distribution of N, S, and I measured with nanoSIMS: a new challenge for element-ratio-based paleoproxies? *Frontiers in Earth Science*, *7*, p.175.

Gruzensky, P.M., 1967. Growth of calcite crystals. J. Phys. Chem. Solids S1, 365–367.

Hemming, N.G., Reeder, R.J., Hart, S.R., 1998. Growth-step-selective incorporation of boron on the calcite surface. Geochim. Cosmochim. Acta 62, 2915–2922.

Hofmann, S., Voïtchovsky, K., Spijker, P., Schmidt, M. and Stumpf, T., 2016. Visualising the molecular alteration of the calcite (104)–water interface by sodium nitrate. *Scientific reports*, *6*(1), 21576.

Jenkins, H.D.B. and Thakur, K.P., 1979. Reappraisal of thermochemical radii for complex ions. Journal of Chemical Education, 56(9), 576.

Kontrec, J., Kralj, D., Brečević, L., Falini, G., Fermani, S., Noethig-Laslo, V. and Mirosavljević, K., 2004. Incorporation of inorganic anions in calcite. *European Journal of Inorganic Chemistry*, *2004*(23), 4579–4585.

Lemarchand, D., Wasserburg, G.J. and Papanastassiou, D.A., 2004. Rate-controlled calcium isotope fractionation in synthetic calcite. Geochimica et cosmochimica acta, 68(22), 4665–4678.

Lueders-Dumont J.A., Forden A.G., Kast E.R., Mohan J.A., Walther B.D., Sigman D.M., Ward B.B. (2022) Controls on the nitrogen isotopic composition of fish otolith organic matter: Lessons from a controlled diet switch experiment, Geochimica et Cosmochimica Acta, 316, 69–86, https://doi.org/10.1016/j.gca.2021.09.030.

Ma, R., Li, K., Guo, Y., Zhang, B., Zhao, X., Linder, S., Guan, C., Chen, G., Gan, Y. and Meng, J., 2021. Mitigation potential of global ammonia emissions and related health impacts in the trade network. *Nature Communications*, *12*(1), 6308.

Matiatos, I., Wassenaar, L.I., Monteiro, L.R., Venkiteswaran, J.J., Gooddy, D.C., Boeckx, P., Sacchi, E., Yue, F.-J., Michalski, G., Alonso-Hern´andez, C., Biasi, C., Bouchaou, L., Edirisinghi, N.V., Fadhullah, W., Fianko, J.R., García-Moya, A.,

Kazakis, N., Li, S.-L., Luu, M.T.N., Priyadarshanee, S., Re, V., Rivera, D.S., Romanelli, A., Sanyal, P., Tamooh, F., Trinh, D.A., Walters, W., Welti, N., 2021. Global patterns of nitrate isotope composition in rivers and adjacent aquifers reveal reactive nitrogen cascading. Commun. Earth Environ. https://doi.org/10.1038/ s43247-021-00121-x.

Mukkamala, S.B., Anson, C.E. and Powell, A.K., 2006. Modelling calcium carbonate biomineralisation processes. Journal of inorganic biochemistry, 100(5-6), 1128–1138.

Paquette, J. and Reeder, R.J., 1995. Relationship between surface structure, growth mechanism, and trace element incorporation in calcite. Geochimica et Cosmochimica acta, 59(4), 735–749.

Schaible, M.J., Castañeda, A.D., Menor-Salvan, C., Pasek, M.A., Burcar, B.T. and Orlando, T.M., 2023. CaCO3 polymorphs as mineral catalysts for prebiotic phosphorylation of uridine. *Earth and Space Science*, *10*, p.e2022EA002577.

Sun, C.Y., Marcus, M.A., Frazier, M.J., Giuffre, A.J., Mass, T., and Gilbert, P.U., 2017. Spherulitic growth of coral skeletons and synthetic aragonite: nature's three-dimensional printing. ACS nano, 11(7), 6612–6622.

Vitousek, P.M., Aber, J.D., Howarth, R.W., Likens, G.E., Matson, P.A., Schindler, D.W., Schlesinger, W.H., Tilman, D.G., 1997. Technical report: Human alteration of the global nitrogen cycle: sources and consequences. Ecol. Appl. 7 (3), 737–750.

Watson, E.B. (2004) A conceptual model for near-surface kinetic controls on the trace element and stable isotope composition of abiogenic calcite crystals. Geochim. Cosmochim. Acta 68, 1473–1488.

Weiner, S. and Addadi, L., 2011. Crystallization pathways in biomineralization. Annual review of materials research, 41(1), 21–40.

Wired Chemist, 2021. Atomic and ionic radii. Available at: http://www.wiredchemist.com/chemistry/data/atomic-and-ionic-radii (accessed 6th August 2020).

Wood, R.S., Chakoumakos, B.C., Fortner, A.M., Gillies-Rector, K., Frontzek, M.D., Ivanov, I.N., Kah, L.C., Kennedy, B., and Pracheil, B.M., 2022. Quantifying fish otolith mineralogy for trace-element chemistry studies. *Scientific Reports*, *12*(1), p.2727.

Wynn, P.M., Fairchild, I.J., Frisia, S., Spötl, C., Baker, A. and Borsato, A., 2010. High-resolution sulphur isotope analysis of speleothem carbonate by secondary ionisation mass spectrometry. Chemical Geology, 271(3-4), 101–107.

Wynn P.M., Fairchild I.J., Borsato A., Spötl C., Hartland A., Baker A., Frisia S., Baldini J.U. (2018) Sulphate partitioning into calcite: Experimental verification of pH control and application to seasonality in speleothems. Geochim. Cosmochim. Acta, 226, 69–83.

Wynn P.M., Ambler S., Grefe I., Soto D.X., Surridge B.W.J., Gabitov R.I., Barker P.A., Anwar J., Quin A., Pereira M.G., and Grant H.K. (2021) Contemporary systematics of vadose zone nitrate capture by speleothem carbonate *Chemical Geology*, 571, 120170, https://doi.org/10.1016/j.chemgeo.2021.120172.

Yamazaki, A., Watanabe, T., Takahata, N., Sano, Y. and Tsunogai, U., 2013. Nitrogen isotopes in intra-crystal coralline aragonites. *Chemical Geology*, *351*, 276–280.

Zhang, Z.M., Chen, S. and Liang, Y.Z., 2010. Baseline correction using adaptive iteratively reweighted penalized least squares. *Analyst*, *135*(5),1138–1146.

Zhao, H., Chen, J., Liu, C., Shen, W., Cai, C. and Ren, Y., 2015. Solubility of calcium carbonate in ammonium chloride aqueous solution at T=(298.15, 323.15, and 348.15) K. Journal of Chemical & Engineering Data, 60(11), 3201–3208.